2538
doi:10.1017/S143192762100903X
Microsc. Microanal. 27 (Suppl 1), 2021

Investigating Space Weathering Effects on Carbonaceous Asteroids Using High-flux and Low-flux Ion Irradiation of the Murchison Meteorite

Dara Laczniak[1], Michelle Thompson[2], Roy Christoffersen[3], Catherine Dukes[4], Simon Clemett[3], Richard Morris[5] and Lindsay Keller[5]

[1]Purdue University - Department of Earth, Atmospheric, and Planetary Sciences, Lafayette, Indiana, United States, [2]Purdue University - Department of Earth, Atmospheric, and Planetary Sciences, United States, [3]Jacobs JETS, NASA Johnson Space Center, United States, [4]University of Virginia, Charlottesville, Virginia, United States, [5]NASA Johnson Space Center, United States

Introduction: Airless planetary bodies are continuously altered by space weathering processes such as solar wind irradiation and micrometeoroid bombardment. These processes change the microstructural, chemical, and optical properties of planetary regoliths and, in turn, complicate interpretations of surface composition from remote sensing data. Previous space weathering investigations have focused primarily on lunar and ordinary chondrite materials, the latter of which have been linked to S-type asteroids [1]. However, relatively little is known about space weathering of primitive carbonaceous chondrites, which contain a combination of hydrous silicate and organic phases and are hypothesized to be fragments of C-complex asteroids [2]. To address this knowledge gap and maximize the science return of missions targeting C-complex asteroids (e.g., NASA OSIRIS-REx targeting Bennu and JAXA Hayabusa2 targeting Ryugu) [3-4], we examine the spectral, microstructural, and chemical effects of simulated solar wind weathering on a carbonaceous asteroid analog material. Here, we present the results from coordinated analyses of Murchison (CM2) meteorite slabs irradiated with 1 keV/amu H^+ and He^+ ions.

Methods: Dry-cut Murchison slabs were exposed to 1 keV H^+ and 4 keV He^+ irradiation under ultra-high vacuum (10^{-8} Pa). For the first set of experiments, we used a high ion flux of ~$1.0x10^{13}$ ions/cm^2/s. H^+-irradiation reached a total fluence of $8.1x10^{17}$ H^+/cm^2 (~700 yrs exposure at Bennu) while He^+-irradiation reached a total fluence of $1.1x10^{18}$ He^+/cm^2 (~23,000 yrs at Bennu). For the second set, we used lower ion fluxes—$6.6x10^{11}$ $H^+/cm^2/s$ and $3.6x10^{11}$ $He^+/cm^2/s$—to more closely simulate the ion flux of actual solar wind (10^8 ions/cm^2/s). H^+-irradiation reached a total fluence of $4.0x10^{16}$ H^+/cm^2 (~20 yrs at Bennu) while He^+-irradiation reached a total fluence of $2.1x10^{16}$ He^+/cm^2 (~400 yrs at Bennu). To characterize the unirradiated, H^+-irradiated, and He^+-irradiated surfaces, we perform five coordinated analytical techniques. Changes in surface chemistry are observed with *in situ* X-ray photoelectron spectroscopy (XPS) using a PHI Versaprobe III Scanning XPS. Changes in spectral slope, surface albedo, and absorption band strengths are evaluated using visible to near-infrared spectra (VNIR; 0.35 – 2.50 µm) acquired with a fiber-optic ASD FieldSpec 3 Spectrometer. Modifications to organic chemistry are investigated using microprobe two-step laser-desorption mass spectrometry (µL^2MS). For transmission electron microscopy (TEM), we prepare four electron transparent cross sections consisting of matrix material, Mg-rich olivine, Fe-rich olivine, and pyroxene, respectively, from each H^+- and He^+-irradiated region using a Quanta 3D DualBeam field emission focused ion beam scanning electron microscope. Lastly, we use a JEOL 2500SE 200 kV field-emission scanning transmission electron microscope equipped with a 60 mm^2 ultra-thin window silicon drift energy dispersive X-ray (EDX) detector to examine the microstructure and composition of ion-affected rims in each FIB-section.

Results: Analyses of low-flux samples is underway, so the following discussion focuses on results from high-flux experiments only. XPS results are consistent with the removal of surface carbon and the chemical reduction of iron from ion irradiation. μL^2MS analyses indicate that He^+-irradiation decreases bulk organic content while H^+-irradiation increases the abundance of some low-molecular-weight free organic species. Absolute reflectance spectra indicate that He^+-irradiation causes spectral brightening and reddening (i.e., increasing reflectance with increasing wavelength) while H^+-irradiation causes only minor reddening.

TEM analysis of the He^+- and H^+-irradiated matrix FIB-sections reveals highly vesiculated ion-affected layers that are ~100 nm and ~50 nm thick, respectively. High-resolution TEM (HRTEM) indicates that phyllosilicate amorphization extends to a depth of ~150 nm below the surface in the He^+-irradiated FIB-section and ~65 nm in the H^+-irradiated FIB-section (Fig. 1). Nanoparticles were observed in localized areas of the He^+-irradiated matrix sample. In the He^+- and H^+-irradiated Mg-rich olivine FIB-sections, ion-affected regions are 65-85 nm and 50-85 nm thick, respectively, characterized by moderate vesiculation, and contain both amorphous and polycrystalline material. The He^+-irradiated Fe-rich olivine FIB-section exhibits a highly vesiculated, completely amorphous ion-affected region (120-180 nm thick). Similar to some Itokawa olivine and low-Ca pyroxene grains, the ion-affected region of our H^+-irradiated Fe-rich olivine FIB-section (~60-75 nm thick) displays only minor vesiculation and consists of three microstructurally/chemically distinct zones (Fig. 2) [5-6]. TEM analysis of the high-flux pyroxene FIB-sections is currently in progress.

Discussion: Results from this study demonstrate that solar wind space weathering of carbonaceous materials is a complex process. Spectral reddening observed in the He^+- and H^+-irradiated spectra may result from the decomposition of phyllosilicates, partial chemical reduction of Fe^{3+} and Fe^{2+}, and subsequent formation of reduced Fe-bearing amorphous material [7-9]. Regarding organic content, He^+- and H^+-irradiation have opposing effects. He^+-irradiation destroys organic material by breaking carbon bonds and sputtering constituent atoms/molecules. Alternatively, H^+-irradiation likely breaks apart large macromolecular organic species into smaller molecular fragments that can be readily detected by the μL^2MS instrument [10]. Microstructurally, the ion-affected regions of our He^+- and H^+-irradiated FIB-sections exhibit varying degrees of vesiculation and structural disorder. Similar to space weathered rims of Itokawa particles [4-5], olivine surfaces from this study tend to exhibit partial amorphization, suggesting that a similar microstructure may be observed in returned regolith grains from asteroids Bennu and Ryugu.

https://doi.org/10.1017/S143192762100903X Published online by Cambridge University Press

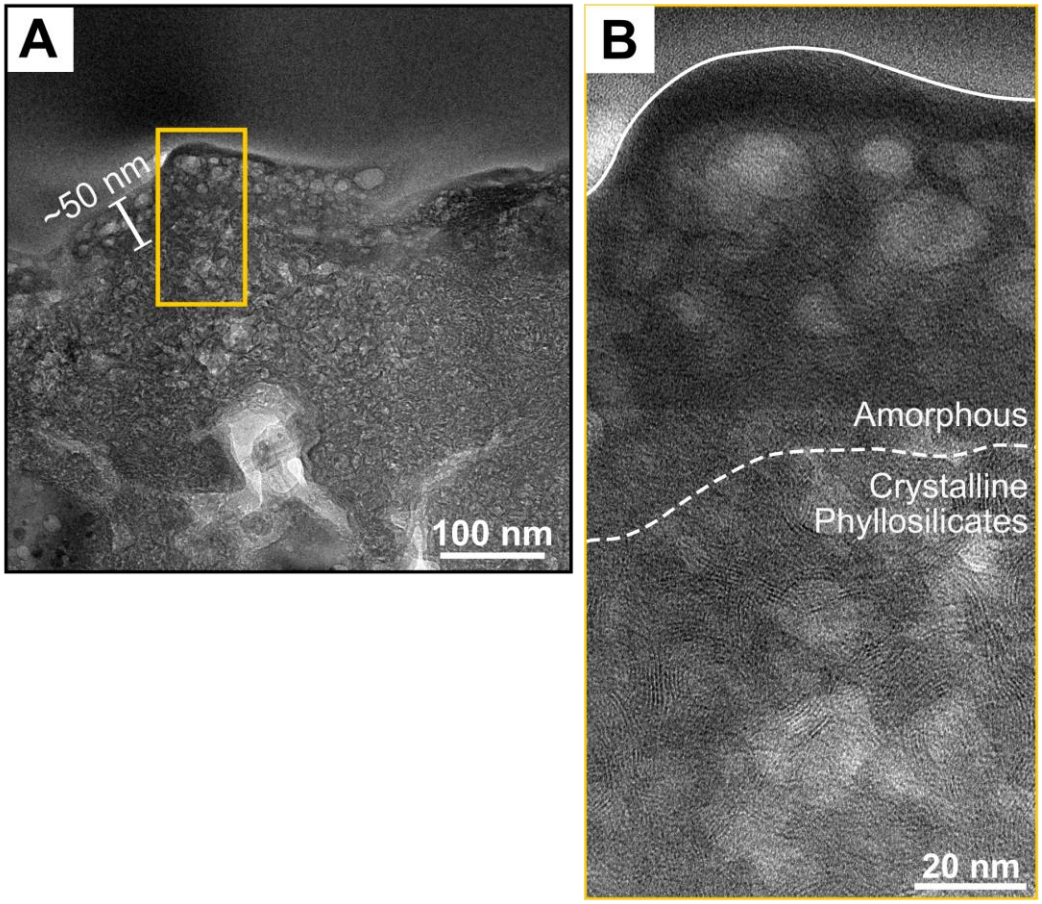

Figure 1. (A) TEM image of the H+-irradiated matrix FIB-section showing the thickness of the vesiculated region (white bracket). (B) HRTEM image of the yellow box in (A) showing a phyllosilicate amorphization depth of ~60-70 nm (dashed white line).

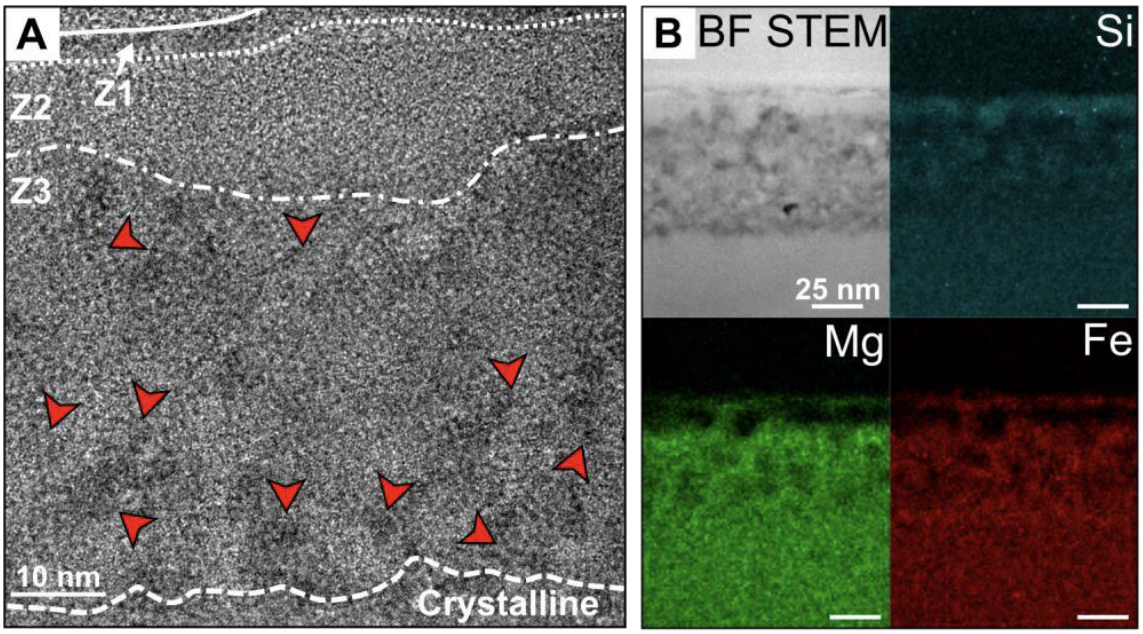

https://doi.org/10.1017/S143192762100903X Published online by Cambridge University Press

Figure 2. (A) HRTEM image showing three microstructurally distinct zones (Z1, Z2, and Z3) in the ion-processed surface of the H+-irradiated Fe-rich olivine FIB-section. Red arrows indicate areas of polycrystallinity. (B) Quantitative Si (cyan), Mg (green), and Fe (red) EDX maps of the region shown in the BF STEM image (upper left). Note that the three microstructural zones shown in (A) also are chemically distinct.

References

[1] Nakamura T. et al. (2011) *Science 333*, 1113-1116
[2] Pieters C.M. & Noble S.K. (2016) *J. Geophys. Res. Planets 121*(10), 1865-1884.
[3] Lauretta D.S. et al. (2017) *Space Sci. Rev. 212*, 925-984.
[4] Watanabe S. et al. (2017) *Space Sci. Rev. 208*, 3-16.
[5] Noguchi T. et al. (2014) *Meteorit. Planet. Sci. 49*(2), 188-214.
[6] Thompson M.S. et al. (2014) *Earth, Planets & Space 66*, 89.
[7] Hapke B. (2001) *J. Geophys. Res. 106*, 10039-10073.
[8] Cloutis E.A. (2015) *46th LPSC*, #1234.
[9] Keller L.P. et al. (2015*) 46th LPSC*, #1913.
[10] Thompson M.S. et al. (2020) *Icarus 346*, 113775.
*This research was supported by NASA grant 80NSSC19K0960.

https://doi.org/10.1017/S143192762100903X Published online by Cambridge University Press